Inorg. Chem. **2004**, *43*, 1840–1849

The First Enantiomerically Pure Helical Noncovalent Tripod for Assembling Nine-Coordinate Lanthanide(III) Podates

Martine Cantuel,[†] Gérald Bernardinelli,[‡] Gilles Muller,[§] James P. Riehl,[§] and Claude Piguet*[,†]

Department of Inorganic, Analytical and Applied Chemistry, University of Geneva, 30 Quai E. Ansermet, CH-1211 Geneva 4, Switzerland, Laboratory of X-ray Crystallography, University of Geneva, 24 Quai E. Ansermet, CH-1211 Geneva 4, Switzerland, and Department of Chemistry, University of Minnesota—Duluth, Duluth, Minnesota 55812-3020

Received November 8, 2003

Decomplexation of the trivalent lanthanide, Ln(III), from the racemic bimetallic triple-stranded helicates $[LnCr(L8)_3]^{6+}$ provides the inert chiral tripodal nonadentate receptor $[Cr(L8)_3]^{3+}$. Elution of the latter podand with $Na_2Sb_2[(+)\text{-}C_4O_6H_2]_2\cdot 5H_2O$ through a cation exchange column allows its separation into its inert helical enantiomers $M\text{-}(+)_{589}\text{-}[Cr(L8)_3]^{3+}$ and $P\text{-}(-)_{589}\text{-}[Cr(L8)_3]^{3+}$, whose absolute configurations are assigned by using CD spectroscopy and exciton theory. Recombination with Ln(III) restores the original triple-stranded helicates $[LnCr(L8)_3]^{6+}$, and the associated thermodynamic parameters unravel the contribution of electrostatic repulsion and preorganization to the complexation process. Combining $M\text{-}(+)_{589}\text{-}[Cr(L8)_3]^{3+}$ with Eu(III) produces the enantiomerically pure d–f helicate $MM\text{-}(-)_{589}\text{-}[EuCr(L8)_3](CF_3SO_3)_6\cdot 4CH_3CN$, whose X-ray crystal structure ($EuCrC_{113}H_{111}N_{25}O_{21}S_6F_{18}$, monoclinic, $P2_1$, $Z = 2$) unambiguously confirms the absolute left-handed configuration for the final helix. The associated ligand-centered and metal-centered chiro-optical properties recorded for the complexes $MM\text{-}[LnCr(L8)_3]^{6+}$ and $PP\text{-}[LnCr(L8)_3]^{6+}$ (Ln = Eu, Gd, Tb) show a strong effect of helicity on specific rotary dispersions, CD and CPL spectra.

Introduction

Since the tuning of metal-centered electronic properties of trivalent lanthanides, Ln(III), in coordination complexes relies on weak crystal-field effects induced by the bound donor atoms,[1] much effort has been focused on the design of covalent tripods fitted with three unsymmetrical tridentate binding units for organizing nonadentate binding sites.[2−8] Upon reaction with Ln(III), the three strands of each ligand L1−L7 wrap around the metal to provide pseudo-tricapped trigonal prismatic sites in the final complexes $[Ln(Li)]^{3+}$ (i = 3, 4, 6, 7)[4,5,7,8] and $[Ln(Li\text{-}3H)]$ (i = 1, 2, 5).[2,3,6] However, the three wrapped tridentate coordinated units in $[Ln(Li)]^{3+}$ (i = 3, 4) and [Ln(L5-3H)] induce drastic sterical constraints within the short tris(2-aminoethyl)amine (TREN) covalent tripod which limit stability and structural programming.[4−6] On the other hand, the macrocyclic triazacyclononane platform in L1−L2 relaxes the steric strain within the tripod,[2,3] but convergence of the three strands toward a single capping atom requires considerable synthetic efforts for designing long semirigid spacers compatible with helicity as those found in L6−L7 (a sequence of seven atoms separates the apical carbon atom and the first coordinated N-atom).[7,8] In this context, self-assembly processes are valuable alternatives for connecting the three strands to a single atom by using coordinate bonds,[9] and the segmental ligand L8 indeed produces triple-stranded heterobimetallic helicates $HHH\text{-}[LnM(L8)_3]^{5+}$ (M = Fe(II), Co(II), Zn(II))

* Corresponding author. E-mail: Claude.Piguet@chiam.unige.ch.
† Department of Inorganic Chemistry, University of Geneva.
‡ Laboratory of X-ray Crystallography, University of Geneva.
§ University of Minnesota—Duluth.

(1) (a) Parker, D.; Dickins, R. S.; Puschmann, H.; Crossland, C.; Howard, J. A. K. *Chem. Rev.* **2002**, *102*, 1977. (b) Bünzli, J.-C. G.; Piguet, C. *Chem. Rev.* **2002**, *102*, 1897.
(2) (a) Tei, L.; Baum, G.; Blake, A. J.; Fenske, D.; Schröder, M. *J. Chem. Soc., Dalton Trans.* **2000**, 2793. (b) Tei, L.; Blake, A. J.; George, M. W.; Weinstein, J. A.; Wilson, C.; Schröder, M. *Dalton Trans.* **2003**, 1693.
(3) Charbonnière, L. J.; Ziessel, R.; Guardigli, M.; Roda, A.; Sabbatini, N.; Cesario, M. *J. Am. Chem. Soc.* **2001**, *123*, 2436.
(4) Bretonnière, Y.; Wietzke, R.; Lebrun, C.; Mazzanti, M.; Pécaut, J. *Inorg. Chem.* **2000**, *39*, 3499.
(5) Renaud, F.; Piguet, C.; Bernardinelli, G.; Bünzli, J.-C. G.; Hopfgartner, G. *J. Am. Chem. Soc.* **1999**, *121*, 9326.
(6) Senegas, J.-M.; Bernardinelli, G.; Imbert, D.; Bünzli, J.-C. G.; Morgantini, P.-Y.; Weber, J.; Piguet, C. *Inorg. Chem.* **2003**, *42*, 4680.
(7) Koeller, S.; Bernardinelli, G.; Bocquet, B.; Piguet, C. *Chem. Eur. J.* **2003**, *9*, 1062.
(8) Koeller, S.; Bernardinelli, G.; Piguet, C. *Dalton Trans.* **2003**, 2395.
(9) Piguet, C.; Edder, C.; Rigault, S.; Bernardinelli, G.; Bünzli, J.-C. G.; Hopfgartner, G. *J. Chem. Soc., Dalton Trans.* **2000**, 3999.

10.1021/ic035292u CCC: $27.50
Published on Web 02/26/2004

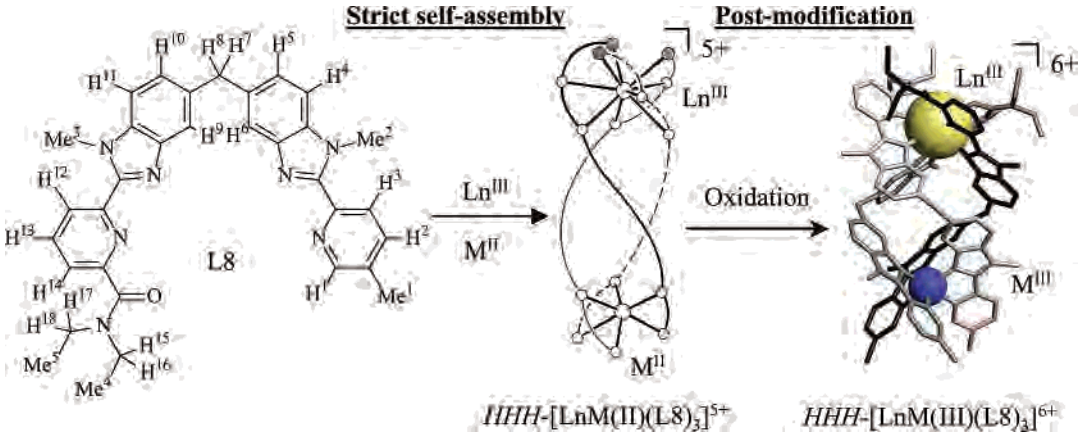

Figure 1. Self-assembly of *HHH*-[LnM(II)(L8)$_3$]$^{5+}$ followed by oxidative post-modification to give the inert noncovalent podates *HHH*-[LnM(III)(L8)$_3$]$^{6+}$ in acetonitrile (M = Co, Cr). The structure on the right corresponds to the X-ray crystal structure of *rac*-[EuCr(L8)$_3$](CF$_3$SO$_3$)$_6$(CH$_3$CN)$_4$ (adapted from ref 12).

Chart 1

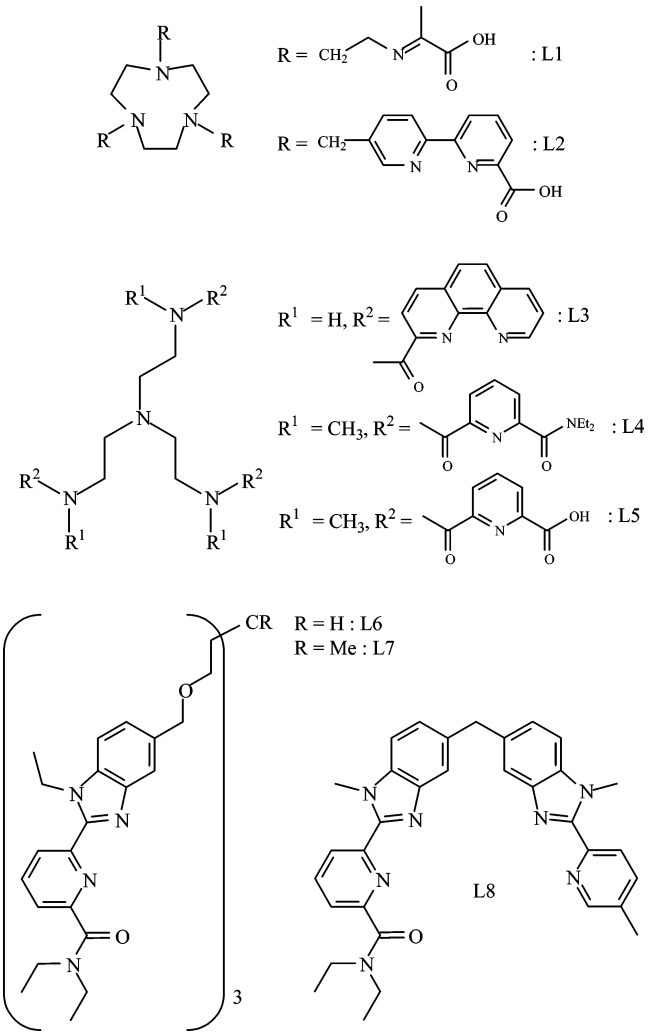

in which the pseudo-octahedral facial [M(2-benzimidazolpyridine)$_3$] fragment acts as a noncovalent tripod which organizes the helical wrapping of the three tridentate *NNO* binding units around Ln(III) (Figure 1).[10] In these noncovalent podates, the Ln(III) coordination site is identical to that found in [Ln(L6)]$^{3+}$ and [Ln(L7)]$^{3+}$, but a chain of eight atoms separates the capping M(II) atom and the first N-atom bound to Ln(III) in *HHH*-[LnM(L8)$_3$]$^{5+}$, which points to the efficiency of the assembly process for organizing sophisticated molecular architectures. However, the lability of the M(II) cations prevents the isolation of the facial receptor *FAC*-[M(L8)$_3$]$^{2+}$ upon decomplexation of Ln(III), and fast rearrangements produce intricate mixtures of complexes.[1b,10] This limitation can be overcome with the use of an inert d-block ion bound in the pseudo-octahedral site, and we have thus explored novel self-assembly processes with oxidative post-modifications in which the labile M(II) ion required for the selective formation of a single helicate during the first step is subsequently transformed into its inert M(III) product (Figure 1).[11,12] Co(II) has been first considered in *HHH*-[LnCo(L8)$_3$]$^{5+}$, but its difficult oxidation into *HHH*-[LnCo(III)(L8)$_3$]$^{6+}$ ($E_{1/2}^{Co(III)/Co(II)} = +0.42$ V vs SCE) leaves traces of Co(II) which catalyze *FAC*-[M(L8)$_3$]$^{3+}$ ⇌ *MER*-[M(L8)$_3$]$^{3+}$ isomerization in solution after removal of the Ln(III) template.[10c,11] The lower reduction potential of [Cr(2,2′-bipyridine)$_3$]$^{3+}$ ($E_{1/2}^{Cr(III)/Cr(II)} = -0.49$ V vs SCE)[13] ensures that Cr(II) is easily and quantitatively oxidized into inert Cr(III), and the successful oxidative post-modification leading to *HHH*-[LnCr(III)(L8)$_3$]$^{6+}$ has been recently described (Figure 1).[12] In this paper we report on the isolation and complexation properties of the noncovalent tripod *FAC*-[Cr(L8)$_3$]$^{3+}$ obtained by decomplexation of Ln(III) from the latter triple-stranded helicates. Since *FAC*-[Cr(L8)$_3$]$^{3+}$ is helical, a special case of chirality,[14] its separation into its right-handed (*P*) and left-handed (*M*) enantiomers has been performed. Special attention has been focused on the structural, thermodynamic, and chiro-optical properties (specific rotary dispersion, CD, CPL) induced by helicity in the

(10) (a) Piguet, C.; Bünzli, J.-C. G.; Bernardinelli, G.; Hopfgartner, G.; Petoud, S.; Schaad, O. *J. Am. Chem. Soc.* **1996**, *118*, 6681. (b) Piguet, C.; Rivara-Minten, E.; Bernardinelli, G.; Bünzli, J.-C. G.; Hopfgartner, G. *J. Chem. Soc., Dalton Trans.* **1997**, 421. (c) Rigault, S.; Piguet, C.; Bernardinelli, G.; Hopfgartner, G. *J. Chem. Soc., Dalton Trans.* **2000**, 4587.
(11) Rigault, S.; Piguet, C.; Bernardinelli, G.; Hopfgartner, G. *Angew. Chem., Int. Ed.* **1998**, *37*, 169.
(12) Cantuel, M.; Bernardinelli, G.; Imbert, D.; Bünzli, J.-C. G.; Hopfgartner, G.; Piguet, C. *J. Chem. Soc., Dalton Trans.* **2002**, 1929.
(13) Baker, B. R.; Mehta, B. D. *Inorg. Chem.* **1965**, *4*, 848.
(14) Cahn, R. S.; Ingold, C.; Prelog, V. *Angew. Chem., Int. Ed. Engl.* **1966**, *5*, 385.

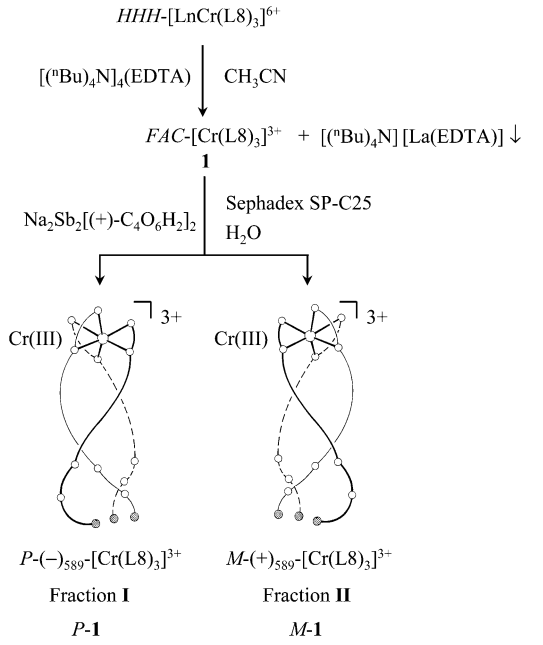

Figure 2. Synthesis of *FAC*-$[Cr(L8)_3]^{3+}$ and separation into its helical enantiomers *M*-$(+)_{589}$-$[Cr(L8)_3]^{3+}$ and *P*-$(-)_{589}$-$[Cr(L8)_3]^{3+}$.

recombinated triple-stranded helicates *MM*-$[LnCr(L8)_3]^{6+}$ and *PP*-$[LnCr(L8)_3]^{6+}$.

Results and Discussion

Preparation and Characterization of the Inert Noncovalent Receptor $[Cr(L8)_3]^{3+}$. Previous ESI-MS, ^{1}H NMR, and luminescence titrations of *HHH*-$[LnCr(III)(L8)_3]^{6+}$ (Ln = La, Eu) with water evidenced that the C_3-symmetrical facial nonadentate receptor *FAC*-$[Cr(L8)_3]^{3+}$ is quantitatively formed for water/acetonitrile ratios $\geq$1:5.[12] Since the heterobimetallic triple-stranded helicates and the nonadentate receptors discussed in this contribution systematically possess a head-to-head-to-head arrangement of the ligand strands, the prefixes *HHH* and *FAC* will be omitted in the rest of our discussion for the sake of simplicity. Isolation on the milligram scale is achieved by treating $[LaCr(III)(L8)_3]^{6+}$ with 1.0 equiv of $[(^nBu)_4N]_4$(EDTA) in acetonitrile, followed by separation (centrifugation) of the insoluble $[(^nBu)_4N]$[La(EDTA)] salt. Precipitation with diethyl ether into the concentrated filtrate provides fair yield (60%) of racemic $[Cr(L8)_3](CF_3SO_3)_3\cdot 4H_2O$ (**1**) (Figure 2).

Decomplexation of La(III) from the nine-coordinate site in **1** is evidenced in the solid state by the 40 cm^{-1} blue shift of the CO stretching vibrations of the carboxamide group when going from $[LaCr(L8)_3](CF_3SO_3)_6$ (ν_{CO} = 1589 cm^{-1})[12] to $[Cr(L8)_3](CF_3SO_3)_3$ (ν_{CO} = 1629 cm^{-1}; ν_{CO} = 1631 cm^{-1} in the free ligand L8).[10a] In solution, the ESI-MS spectrum of **1** shows the expected peaks corresponding to $[Cr(L8)_3(CF_3SO_3)_x]^{(3-x)+}$ (x = 0−2, Figure S1, Supporting Information), and the ^{1}H NMR spectrum points to the formation of a single C_3-symmetrical complex displaying 14 signals severely broadened by the slow-relaxing Cr(III) center ($\tau_e \approx 10^{-9}$ s, Figure 3a).[15] Interestingly, the paramagnetic contributions to the chemical shifts are negligible for the protons H12−H18 and Me3−Me5 which are sufficiently remote from the Cr(III) center (see Figure 1 for the numbering scheme). Comparison with the NMR spectrum of the free ligand L8 thus allows a straightforward assignment (Figure 3b). On the other hand, the signals of the protons close (H7−H11) or attached (H1−H6, Me1−Me2) to the coordinated bidentate binding units are severely paramagnetically broadened and shifted and cannot be unambiguously assigned (Figure 3).

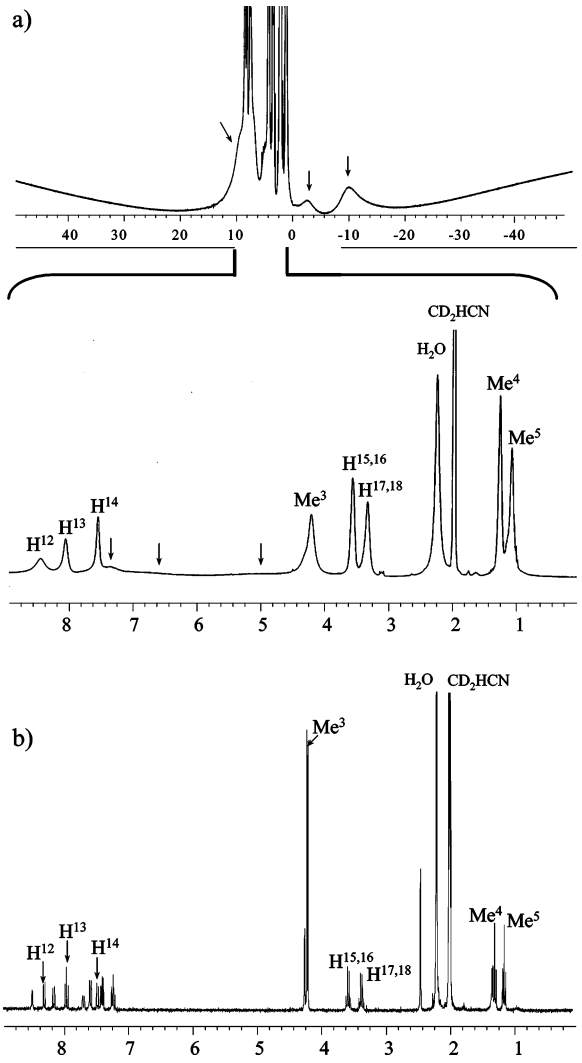

Figure 3. 300 MHz ^{1}H NMR spectrum of (a) $[Cr(L8)_3]^{3+}$ and (b) L8 in CD_3CN (298 K, the arrows highlight broad and paramagnetically shifted signals of protons bound to the bidentate binding unit in $[Cr(L8)_3]^{3+}$).

Finally, the absorption spectrum of **1** in acetonitrile shows the characteristic and intense ligand-centered $\pi \rightarrow \pi^*$ transitions at 31 150 cm^{-1} together with weaker bands appearing on the low-energy side and previously assigned to a combination of the charge transfer (CT) and the Cr-centered spin-allowed $^4A_2 \rightarrow {}^4T_1 + {}^4T_2$ transitions (25 700−21 600 cm^{-1}, Figure 4).[12] Compared with the absorption spectrum of $[LaCr(L8)_3]^{6+}$,[12] the decomplexation of La(III) mainly results in a 1500 cm^{-1} blue shift of the maximum of the band envelope of the $\pi \rightarrow \pi^*$ transitions in $[Cr(L8)_3]^{3+}$, a change which will be exploited for exploring the thermodynamic recombination process (Figure 5).

(15) Bertini, I.; Luchinat, C. *Coord. Chem. Rev.* **1996**, *150*, 77.

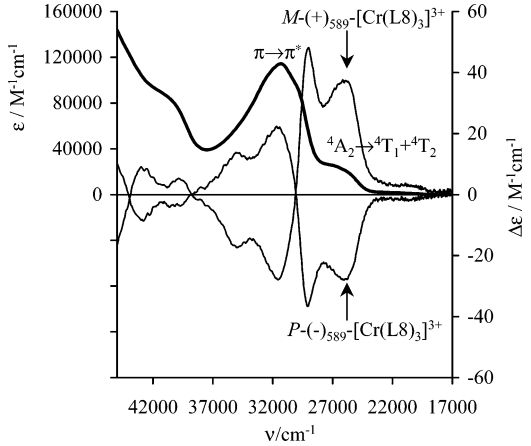

Figure 4. Absoprtion spectrum of $[Cr(L8)_3]^{3+}$ (bold line) and circular dichroism spectra of *M*-$(+)_{589}$-$[Cr(L8)_3]^{3+}$ (*M*-**1**) and *P*-$(-)_{589}$-$[Cr(L8)_3]^{3+}$ (*P*-**1**, acetonitrile, 5×10^{-5} M).

Separation of $[Cr(L8)_3]^{3+}$ into its Helical Enantiomers *M*-$(+)_{589}$-$[Cr(L8)_3]^{3+}$ and *P*-$(-)_{589}$-$[Cr(L8)_3]^{3+}$. The racemic receptor *rac*-$[Cr(L8)_3]^{3+}$ was sorbed onto a Sephadex SP-C25 ion-exchange resin and eluted with 0.15 M aqueous solution of $Na_2Sb_2[(+)\text{-}C_4O_6H_2]_2 \cdot 5H_2O$.[16] Two successive orange bands can be separated leading to fractions I (shortest retention time) and II (longest retention time). Extraction with dichloromethane in the presence of sodium triflate provides approximately equal quantities of the two enantiomers $(-)_{589}$-$[Cr(L8)_3](CF_3SO_3)_3$ (fraction I, yield: 45%) and $(+)_{589}$-$[Cr(L8)_3](CF_3SO_3)_3$ (fraction II, yield: 41%) displaying respective specific rotary dispersions of $[\alpha]_{589}^{20} = -782(20)$ and $[\alpha]_{589}^{20} = +828(21)$ deg·mol^{-1}·dm^2.[17] Identical results are obtained when the Sephadex column was sorbed with $[LaCr(L8)_3]^{6+}$ because La(III) is quantitatively decomplexed in aqueous solution. As expected, the circular dichroism (CD) spectra of the two fractions are mirror images and display strong Cotton effects for the seven transitions detected in the 20 000−45 000 cm^{-1} range (Figure 4).

According to the exciton theory applied to D_3-symmetrical $[M(2,2'\text{-bipyridine})_3]^{n+}$ and $[M(1,10\text{-phenanthroline})_3]^{n+}$ complexes, three long-axis-polarized ligand-centered $\pi \rightarrow \pi^*$ transitions ($\Psi_0 \rightarrow \Psi_{E1}$, $\Psi_0 \rightarrow \Psi_{E2}$, and $\Psi_0 \rightarrow \Psi_{A2}$) produce helical movements of the electrons which induce two strong CD signals in the near-UV since $\Psi_0 \rightarrow \Psi_{E1}$ and $\Psi_0 \rightarrow \Psi_{E2}$ are degenerate.[18] Experimental data for *M*-$(-)_{589}$-$[Fe(phen)_3]^{2+}$, whose absolute configuration has been determined by X-ray diffraction,[19] display a negative CD signal occurring at high energy (38 500 cm^{-1}) for the $\Psi_0 \rightarrow \Psi_{A2}$ transition, and a positive signal occurring at lower energy for the $\Psi_0 \rightarrow \Psi_E$ transition (36 800 cm^{-1}).[20] These observations are further corroborated for *M*-$(+)_{589}$-$[Cr(phen)_3]^{3+}$ which displays a very similar pattern ($\Psi_0 \rightarrow \Psi_{A2}$ at 38 600 cm^{-1}with $\Delta\epsilon = -105$ M^{-1} cm^{-1} and $\Psi_0 \rightarrow \Psi_E$ at 36 500 cm^{-1} with $\Delta\epsilon = +145$ M^{-1} cm^{-1}) and for *M*-$(+)_{589}$-$[Cr(bipy)_3]^{3+}$ ($\Psi_0 \rightarrow \Psi_{A2}$ at 34 500 cm^{-1}with $\Delta\epsilon = -8$ M^{-1}cm^{-1} and $\Psi_0 \rightarrow \Psi_E$ at 31 900 cm^{-1} with $\Delta\epsilon = +50$ M^{-1}cm^{-1}).[21] Straightforward comparisons with the related splitting observed for the $\pi \rightarrow \pi^*$ transitions (barycenter: 31 150 cm^{-1}) in the CD spectrum of $(+)_{589}$-$[Cr(L8)_3]^{3+}$ occurring at 31 750 cm^{-1} ($\Delta\epsilon = -22$ M^{-1} cm^{-1} assigned to $\Psi_0 \rightarrow \Psi_{A2}$) and 29 070 cm^{-1} ($\Delta\epsilon = +48$ M^{-1} cm^{-1} assigned to $\Psi_0 \rightarrow \Psi_E$) strongly suggest the existence of the left-handed helix *M*-$(+)_{589}$-$[Cr(L8)_3]^{3+}$ (Figure 4). However, the splitting between the A_2 and E levels is small, and their relative energies depend on subtle effects induced by the trigonal field ($[Cr(L8)_3]^{3+}$ exhibits only C_3-symmetry compared with D_3-symmetry for $[Cr(bipy)_3]^{3+}$), and the excitation resonance interactions in each specific complex.[21] It is therefore difficult to eventually assign the absolute configurations of $[Cr(L8)_3]^{3+}$ based on the exclusive comparisons with the near-UV CD spectra of $[Cr(phen)_3]^{3+}$ and $[Cr(bipy)_3]^{3+}$, but the reliable absolute left-handed configuration determined from the X-ray crystal structure of *MM*-$[EuCr(L8)_3]^{6+}$ obtained upon recombination of $(+)_{589}$-$[Cr(L8)_3]^{3+}$ with Eu(III) (vide infra) unambiguously confirms that $E(\Psi_0 \rightarrow \Psi_{A2}) > E(\Psi_0 \rightarrow \Psi_E)$ in $[Cr(L8)_3]^{3+}$ as in $[Cr(phen)_3]^{3+}$ and $[Cr(bipy)_3]^{3+}$, thus leading to the definitive assignments: *P*-$(-)_{589}$-$[Cr(L8)_3]^{3+}$ for fraction I (*P*-**1**) and *M*-$(+)_{589}$-$[Cr(L8)_3]^{3+}$ for fraction II (*M*-**1**, Figure 2). Since we do not record CD spectra for concentrated solutions, the weak spin-forbidden Cr($^4A_2 \rightarrow {}^2T_1, {}^2E$) transitions escape detection, but the positive CD signal recorded for the spin-allowed Cr($^4A_2 \rightarrow {}^4T_2$) transition at 21 500 cm^{-1} ($\Delta\epsilon = +1.8$ M^{-1} cm^{-1}) in *M*-$(+)_{589}$-$[Cr(L8)_3]^{3+}$ (Figure 4) matches a similar behavior reported for *M*-$(+)_{589}$-$[Cr(phen)_3]^{3+}$ (21 900 cm^{-1}, $\Delta\epsilon = +2.5$ M^{-1} cm^{-1}).[22] Finally, the strong positive Cotton effect centered at 26 500 cm^{-1} for *M*-$(+)_{589}$-$[Cr(L8)_3]^{3+}$ and corresponding to the combination of CT and Cr($^4A_2 \rightarrow {}^4T_1$) transitions occurring in this domain[12] has its exact counterpart in *M*-$(+)_{589}$-$[Cr(bipy)_3]^{3+}$ (29 000 cm^{-1})[21] and *M*-$(+)_{589}$-$[Cr(phen)_3]^{3+}$ (31 000 cm^{-1}),[22] but no detailed discussion of its origin has been given.[21,22]

In conclusion, the CD spectra observed for *M*-$(+)_{589}$-$[Cr(L8)_3]^{3+}$, *M*-$(+)_{589}$-$[Cr(bipy)_3]^{3+}$, and *M*-$(+)_{589}$-$[Cr(phen)_3]^{3+}$[21-22] display the same alternance of Cotton effects except for a blue shift of the barycenters of the $\pi \rightarrow \pi^*$ and CT transitions when going from coordinated 2-benzimidazolyl-pyridine ligands to 2,2′-bipyridine ($\Delta E \approx 3000$ cm^{-1}) and 1,10-phenanthroline ($\Delta E \approx 6000$ cm^{-1}). It is also worth noting that the optical activity of solutions of *M*-$(+)_{589}$-$[Cr(L8)_3]^{3+}$, or of *P*-$(-)_{589}$-$[Cr(L8)_3]^{3+}$ (5×10^{-5} M in acetonitrile), does not change for one month at room temperature in agreement with the well-established inertness of Cr(III) complexes.[23]

Recombination of $[Cr(L8)_3]^{3+}$ with $Ln(CF_3SO_3)_3$ (Ln = La−Lu). Spectrophotometric titrations of racemic [Cr-

(16) Yoshikawa, Y.; Yamasaki, K. *Coord. Chem. Rev.* **1979**, *28*, 205.
(17) March, J. *Advanced Organic Chemistry*, 4th ed.; John Wiley & Sons: New York, 1992; p 96.
(18) Bosnich, B. *Acc. Chem. Res.* **1969**, *2*, 266.
(19) Templeton, D. H.; Zalkin, A.; Ueki, T. *Acta Crystallogr., Suppl. A* **1966**, *21*, 154.
(20) McCaffery, A. J.; Mason, S. F.; Norman, B. J. *J. Chem. Soc. A* **1969**, 1428.
(21) (a) Ferguson, J.; Hawkins, C. J.; Kane-Maguire, L. A. P.; Lip, H. *Inorg. Chem.* **1969**, *8*, 771. (b) Mason, S. F.; Peart, B. J.; Waddell, R. E. *J. Chem. Soc., Dalton Trans.* **1973**, 944. (c) Mason, S. F.; Peart, B. J. *J. Chem. Soc., Dalton Trans.* **1973**, 949.
(22) (a) Kaizaki, S.; Hidaka, J.; Shimura, Y. *Bull. Chem. Soc. Jpn.* **1970**, *43*, 1100. (b) Kaizaki, S.; Hidaka, J.; Shimura, Y. *Inorg. Chem.* **1973**, *12*, 142.

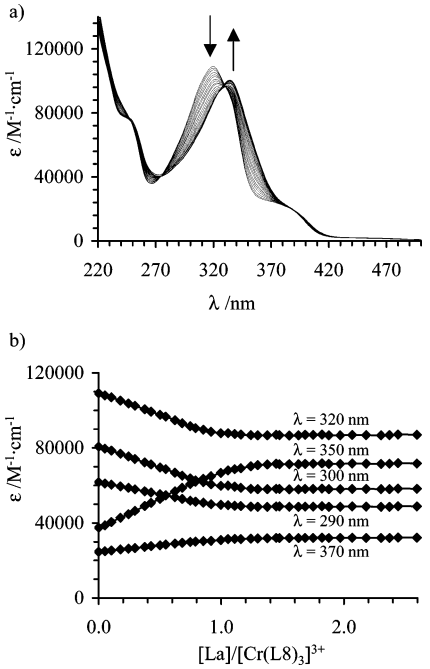

Figure 5. (a) Variation of absorption spectra observed for the spectrophotometric titration of *rac*-$[Cr(L8)_3]^{3+}$ (10^{-4} mol·dm^{-3} in acetonitrile) with $La(CF_3SO_3)_3 \cdot 3H_2O$ at 293 K ($La:[Cr(L8)_3]^{3+} = 0.1-2.5$). (b) Corresponding variation of observed molar extinctions at 5 different wavelengths.

Table 1. Formation Constants $\log(\beta_{11}^{Ln})$ for the Complexes $[LnCr(L8)_3]^{6+}$ Obtained from $[Cr(L8)_3]^{3+}$ According to Equation 1 (Acetonitrile, 293 K)

Ln(III)	$\log(\beta_{11}^{Ln})$	Ln(III)	$\log(\beta_{11}^{Ln})$
La(III)	5.9 ± 0.3	Er(III)	5.3 ± 0.3
Nd(III)	5.4 ± 0.3	Lu(III)	5.3 ± 0.3
Gd(III)	5.4 ± 0.3		

$(L8)_3]^{3+}$ (10^{-4} M in acetonitrile) with $Ln(CF_3SO_3)_3 \cdot xH_2O$ (Ln = La, Nd, Gd, Er, Lu; $x = 1-4$) show a smooth evolution of the absorption spectra resulting from the expected 1500 cm^{-1} red shift of the barycenter of the ligand-centered $\pi \rightarrow \pi^*$ transitions occurring upon complexation of the tridentate binding unit to Ln(III) (Figure 5).[12] A single end point is observed for $Ln/[Cr(L8)_3]^{3+} = 1.0$, together with two isosbestic points at 275 and 329 nm implying the existence of only two species ($[Cr(L8)_3]^{3+}$ and $[LnCr(L8)_3]^{6+}$) absorbing in the near UV. The spectrophotometric data can be satisfyingly fitted with nonlinear least-squares techniques to eq 1.[24]

$$Ln^{3+} + [Cr(L8)_3]^{3+} \rightleftharpoons [LnCr(L8)_3]^{6+} \quad \log(\beta_{11}^{Ln}) \qquad (1)$$

The formation constants $\log(\beta_{11}^{Ln}) = 5.3-5.9$ do not vary significantly along the lanthanide series within experimental errors and point to negligible size-discriminating effects (Table 1).

These β_{11}^{Ln} constants are 1−2 orders of magnitude smaller than those obtained for the formation of the podates $[Ln(L6)]^{3+}$ ($\log(\beta_{11}^{Ln}) = 6.5-7.6$)[7] and $[Ln(L7)]^{3+}$ ($\log(\beta_{11}^{Ln}) = 7.2-8.2$)[8] which possess the same nine-coordinate N_6O_3 cavity. At first sight, the reduced affinity of $[Cr(L8)_3]^{3+}$ for Ln(III) can be assigned to the electrostatic repulsion between the entering trivalent lanthanide and the positively charged receptor, compared with the neutral podands L6 and L7. According to a simple electrostatic model considering the metallic centers in the final helicate $[LnCr(L8)_3]^{6+}$ as two triply charged dots separated by $R_{Ln-Cr} = 9.3$ Å (taken from the crystal structures of $[LnCr(L8)_3](CF_3SO_3)_6 \cdot 4CH_3CN$, Ln = Eu, Lu),[12] the electrostatic work W for complexing Ln^{3+} to $[Cr(L8)_3]^{3+}$ is given by eq 2 in which q stands for the electrostatic charge (1.602×10^{-19} C), ϵ_0 is the vacuum permittivity constant (8.8419×10^{-12} C^2 N^{-1} m^{-2}), and ϵ_{rel} is the relative dielectric constant of the medium separating the point charges during the complexation process.[10c,25]

$$W = \frac{9q^2}{4\pi\epsilon_0}\int_{\infty}^{R_{LnCr}} \frac{1}{\epsilon_{rel} r^2}\, dr \qquad (2)$$

When Ln^{3+} and $[Cr(L8)_3]^{3+}$ are well-separated in solution, $\epsilon_{rel} = \epsilon_{acetonitrile} = 36.2$,[26] and this value slightly reduces to reach $\epsilon_{rel} \approx 30$ in $[LnCr(L8)_3]^{6+}$, as previously determined by electrochemical investigations of electron transfer reactions occurring in closely related bimetallic Fe_2[25] and LaCo[10c] triple-stranded helicates in acetonitrile. We have thus used an average constant value of $\epsilon_{rel} \approx 30$ for calculating $W \approx 44.9$ kJ·mol^{-1} with eq 2. This value is much larger than the difference in free energies $\Delta(\Delta G°)$ between the formation of the covalent $[Ln(Li)]^{3+}$ and the noncovalent podates $[LnCr(L8)_3]^{6+}$ ($\Delta(\Delta G°) = \Delta G_f°([Ln(Li)]^{3+}) - \Delta G_f°([LnCr(L8)_3]^{3+}) = 9$ kJ·mol^{-1} for $i = 6$ and $\Delta(\Delta G°) = 13$ kJ·mol^{-1} for $i = 7$) which implies that the expected increased electrostatic repulsion accompanying the formation of $[LnCr(L8)_3]^{6+}$ (eq 1) is partially overcome by other contributions, among which (i) polarization effects which reduce the positive charge borne by the metal ions,[27] (ii) an improved preorganization of the tridentate binding units in $[Cr(L8)_3]^{3+}$, and (iii) a larger increase of the translational entropy accompanying the desolvation of the charged receptor $[Cr(L8)_3]^{3+}$ may be tentatively invoked. Whatever the origin of the reduced repulsive interaction occurring between $[Cr(L8)_3]^{3+}$ and Ln^{3+}, eq 1 provides final helicates which are thus stable enough in acetonitrile to be investigated for their chiro-optical properties, and reactions of *M*-$(+)_{589}$-$[Cr(L8)_3]^{3+}$ (*M*-**1**) and *P*-$(-)_{589}$-$[Cr(L8)_3]^{3+}$ (*P*-**1**), respectively, with $Ln(CF_3SO_3)_3 \cdot xH_2O$ (Ln = Eu, Gd, Tb; $x = 2-4$) produce good yields (77−92%) of *MM*-$(-)_{589}$-$[LnCr(L8)_3](CF_3SO_3)_6 \cdot xH_2O$ (Ln = Eu, $x = 1$, *MM*-**2**; Ln = Gd, $x = 3$, *MM*-**3**; Ln = Tb, $x = 6.5$, *MM*-**4**) and *PP*-$(+)_{589}$-$[LnCr(L8)_3](CF_3SO_3)_6 \cdot xH_2O$ (Ln = Eu, $x = 1.5$, *PP*-**2**; Ln = Gd, $x = 1.5$, *PP*-**3**; Ln = Tb, $x = 8$, *PP*-**4**) after isolation as their triflate salts (Table S1, Supporting Information). Ultra-slow

(23) Lincoln, S. F.; Merbach, A. E. *Adv. Inorg. Chem.* **1995**, *42*, 1.
(24) (a) Gampp, H.; Maeder, M.; Meyer, C. J.; Zuberbühler, A. *Talanta* **1986**, *33*, 943. (b) Gampp, H.; Maeder, M.; Meyer, C. J.; Zuberbühler, A. *Talanta* **1985**, *23*, 1133.
(25) Serr, B. R.; Andersen, K. A.; Elliott, C. M.; Anderson, O. P. *Inorg. Chem.* **1988**, *27*, 4499.
(26) Geary, W. J. *Coord. Chem. Rev.* **1971**, *7*, 81.
(27) (a) Berny, F.; Muzet, N.; Troxler, L.; Dedieu, A.; Wipff, G. *Inorg. Chem.* **1999**, *38*, 1244. (b) Baaden, M.; Berny, F.; Madic, C.; Wipff, G. *J. Phys. Chem. A* **2000**, *104*, 7659. (c) Wipff, G.; Berny, F. *J. Chem. Soc., Perkin Trans. 2* **2001**, 73.

Table 2. Selected Bond Distances (Å) and Angles (deg) for *MM*-[EuCr(L8)$_3$](CF$_3$SO$_3$)$_6$(CH$_3$CN)$_4$ (*MM*-**5**) and *rac*-[EuCr(L8)$_3$](CF$_3$SO$_3$)$_6$(CH$_3$CN)$_4$ (*rac*-**5**)[12]

Distances						
	ligand a		ligand b		ligand c	
	MM-**5**	*rac*-**5**[a]	*MM*-**5**	*rac*-**5**[a]	*MM*-**5**	*rac*-**5**[a]
Eu···Cr	9.217(2)	9.3238(8)				
Eu−O1	2.44(1)	2.422(4)	2.42(1)	2.397(3)	2.355(8)	2.383(3)
Eu−N4	2.60(1)	2.592(4)	2.62(1)	2.575(4)	2.56(1)	2.573(4)
Eu−N6	2.58(1)	2.599(4)	2.58(1)	2.602(4)	2.58(1)	2.624(4)
Cr−N1	2.11(1)	2.073(4)	2.05(1)	2.079(4)	2.08(1)	2.087(4)
Cr−N2	1.98(1)	2.018(4)	2.02(1)	2.027(4)	2.01(1)	2.025(4)
Bite Angles						
	ligand a		ligand b		ligand c	
	MM-**5**	*rac*-**5**[a]	*MM*-**5**	*rac*-**5**[a]	*MM*-**5**	*rac*-**5**[a]
N1−Cr−N2	79.5(4)	79.6(2)	79.1(4)	79.6(1)	78.3(5)	79.4(2)
N4−Eu−N6	61.3(3)	62.1(1)	64.0(4)	62.6(1)	62.6(3)	63.0(1)
N6−Eu−O1	64.1(3)	63.4(1)	64.0(4)	63.7(1)	63.0(3)	63.2(1)
N4−Eu−O1	125.4(4)	125.3(1)	127.9(4)	126.3(1)	125.5(3)	126.1(1)
Angles						
	MM-**5**	*rac*-**5**[a]			*MM*-**5**	*rac*-**5**[a]
N−Cr−N Angles						
N1a−Cr−N2b	87.3(4)	89.0(2)		N1a−Cr−N1c	96.6(4)	95.5(2)
N1a−Cr−N2c	174.3(5)	174.4(2)		N2a−Cr−N1b	171.3(5)	171.3(2)
N2a−Cr−N2b	95.0(4)	97.4(2)		N2a−Cr−N1c	88.9(4)	87.7(2)
N2a−Cr−N2c	97.7(4)	97.8(2)		N1a−Cr−N1b	93.7(4)	92.1(2)
N1b−Cr−N1c	97.4(4)	95.9(2)		N1b−Cr−N2c	89.5(5)	90.8(2)
N2b−Cr−N1c	174.9(5)	173.7(2)		N2b−Cr−N2c	97.9(5)	96.3(2)
N−Eu−N Angles						
N4a−Eu−N4b	86.9(3)	86.1(1)		N6a−Eu−N6b	118.9(4)	121.7(1)
N4b−Eu−N4c	83.5(4)	85.8(1)		N6b−Eu−N6c	119.2(4)	118.7(1)
N4a−Eu−N4c	88.6(3)	88.7(1)		N6a−Eu−N6c	119.7(3)	118.6(1)
N4a−Eu−N6c	148.6(3)	147.6(1)		N4a−Eu−N6b	76.5(3)	75.2(1)
N6a−Eu−N4b	143.7(3)	142.0(1)		N4b−Eu−N6c	78.0(3)	76.9(1)
N6b−Eu−N4c	144.5(4)	145.0(1)		N6a−Eu−N4c	79.0(3)	73.8(1)
O−Eu−N Angles						
O1c−Eu−N4a	142.7(3)	142.6(1)		O1b−Eu−N4a	79.5(3)	78.4(1)
O1b−Eu−N6a	66.5(4)	70.1(1)		O1c−Eu−N6a	132.6(3)	134.2(1)
O1c−Eu−N6b	66.8(3)	68.2(1)		O1c−Eu−N4b	83.1(3)	83.8(1)
O1a−Eu−N6b	131.0(4)	134.1(1)		O1a−Eu−N4b	144.8(3)	145.0(1)
O1a−Eu−N4c	83.8(3)	80.5(1)		O1a−Eu−N6c	67.0(4)	68.1(1)
O1b−Eu−N4c	145.1(4)	143.6(1)		O1b−Eu−N6c	131.2(3)	133.8(1)
O−Eu−O Angles						
O1a−Eu−O1b	76.9(4)	79.8(1)		O(1b)−Eu−O(1c)	78.6(3)	79.0(1)
O1a−Eu−O1c	77.9(3)	78.8(1)				

[a] Taken from ref 12.

diffusion of diethyl ether into a concentrated acetonitrile solution of *MM*-**2** provides fragile crystals of *MM*-(−)$_{589}$-[EuCr(L8)$_3$](CF$_3$SO$_3$)$_6$·4CH$_3$CN (*MM*-**5**) suitable for X-ray diffraction studies.

Crystal and Molecular Structure of *MM*-(−)$_{589}$-[EuCr(L8)$_3$](CF$_3$SO$_3$)$_6$·4CH$_3$CN (*MM*-5). *MM*-**5** crystallizes in the monoclinic crystal system as previously found for the analogous racemic complex [EuCr(L8)$_3$](CF$_3$SO$_3$)$_6$·4CH$_3$CN (*rac*-**5**),[12] but the space group changes from $P2_1/n$ ($Z = 4$) to noncentrosymmetric $P2_1$ ($Z = 2$) when going from *rac*-**5** to *MM*-**5**. The uncoordinated anions and solvent molecules are slightly disordered (see Experimental Section) but show no other feature of interest. The discrete cations [EuCr(L8)$_3$]$^{6+}$ in *MM*-**5** exhibit the expected triple-helical structure in which the two metals define a pseudo-C_3 axis about which the three ligand strands are helically wrapped in a head-to-head-to-head arrangement as previously described in *rac*-**5**.[12] Contrary to *rac*-**5**, the two cations in the unit cell of *MM*-**5** display the same helicity whose absolute configuration is unambiguously assigned to a left-handed helix *MM*-[EuCr(L8)$_3$]$^{6+}$ (Flack parameter:[28] $x = -0.01(1)$). The atomic numbering scheme and a perspective view of the cation *MM*-[EuCr(L8)$_3$]$^{6+}$ are shown in Figure 6, Table 2 collects selected geometrical parameters, and least-squares planes are given in Table S2 (Supporting Information).

The molecular structures of *MM*-[EuCr(L8)$_3$]$^{6+}$ observed in *MM*-**5** are almost superimposable with that previously reported for the *MM* enantiomer contained in *rac*-**5** (Figure S2, Supporting Information), thus leading to similar geometrical parameters (Table 2 and Tables S3−S4, Supporting Information). The intramolecular intermetallic Eu···Cr distance in *MM*-**5** (9.217(2) Å) is marginally smaller than

(28) (a) Flack, H. D.; Bernardinelli, G. *Acta Crystallogr.* **1999**, *A55*, 908. (b) Flack, H. D.; Bernardinelli, G. *J. Appl. Crystallogr.* **2000**, *33*, 1143.

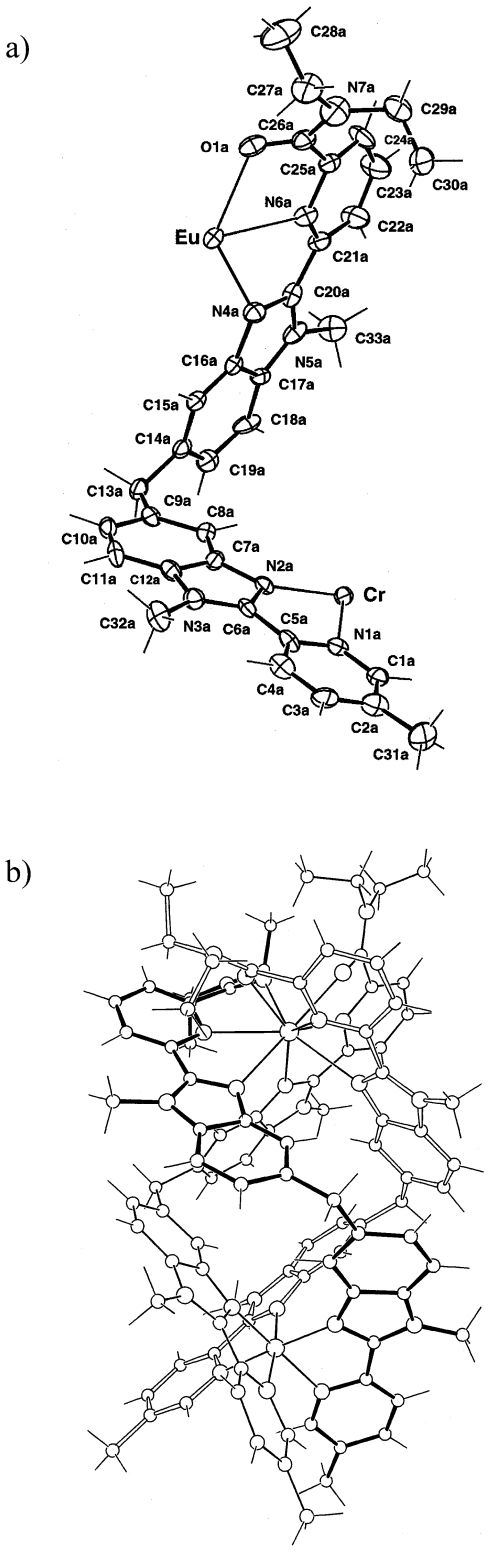

Figure 6. (a) ORTEP view of the coordinated strand *a* showing the atomic numbering scheme. Ellipsoids are represented at 40% probability level. (b) Perspective view of the molecular structure of the cation *MM*-$[EuCr(L8)_3]^{6+}$ approximately perpendicular to the *pseudo*-3-fold axis.

Eu···Cr = 9.3238(8) Å reported for *rac*-**5**, and a detailed analysis of the helical revolution of the strands in both complexes confirm negligible differences of the helical pitches in the two triple helices (Table S5, Supporting Information).[12] Interestingly, the packing of the triple-helical cations $[EuCr(L8)_3]^{6+}$ in the crystal of *MM*-**5** and in *rac*-**5** is also very similar with their *pseudo*-C_3 axis roughly aligned along the [101] direction (deviation: 4.0°) for *MM*-**5**, or along the [100] direction (deviation: 5.7°) for *rac*-**5**,[12] thus forming columns packed in a compact pseudohexagonal arrangement (Figure S3, Supporting Information). Within each column in *MM*-**5**, the orientation of the Eu−Cr vectors and the screw sense are invariant, but adjacent columns show the opposite orientation of the Eu−Cr vector, while the left-handed helicity is obviously maintained. The triflate anions and solvent molecules occupy the interstices between the columns.

Table 3. Specific Rotary Dispersion for the Complexes *M*/*P*-$[Cr(L8)_3]^{3+}$ and *MM*/*PP*-$[LnCr(L8)_3]^{6+}$ (Ln = Eu, Gd, Tb) (10^{-3} M in Acetonitrile, 293 K)

	$[\alpha]_{589}^{20}$/deg·mol^{-1}·dm^2
P-(−)-$[Cr(L8)_3]^{3+}$ (*P*-**1**)	−782(20)
M-(+)-$[Cr(L8)_3]^{3+}$ (*M*-**1**)	830(21)
PP-(+)-$[EuCr(L8)_3]^{6+}$ (*PP*-**2**)	1146(46)
MM-(−)-$[EuCr(L8)_3]^{6+}$ (*MM*-**2**)	−1239(50)
PP-(+)-$[GdCr(L8)_3]^{6+}$ (*PP*-**3**)	1039(42)
MM-(−)-$[GdCr(L8)_3]^{6+}$ (*MM*-**3**)	−892(36)
PP-(+)-$[TbCr(L8)_3]^{6+}$ (*PP*-**4**)	994(40)
MM-(−)-$[TbCr(L8)_3]^{6+}$ (*MM*-**4**)	−979(39)

We can conclude that the rather rigid organization of the ligand strands in $[EuCr(L8)_3]^{6+}$ provides triple-stranded helicates of similar shapes and geometries for both racemic and enantiomerically pure samples. Moreover, the analysis of the X-ray diffraction data unambiguously assigned a left-handed helicity for *MM*-$(-)_{589}$-$[EuCr(L8)_3]^{6+}$ obtained upon reaction of $(+)_{589}$-$[Cr(L8)_3]^{3+}$ with Eu(III) in complete agreement with the original attribution of left-handed helicity for *M*-$(+)_{589}$-$[Cr(L8)_3]^{3+}$ based on the analysis of CD spectra. According to the well-established extreme inertness of the Cr(III) complexes,[23] confirmed by the lack of racemization observed for $(+)_{589}$-$[Cr(L8)_3]^{3+}$ in solution for one month, inversion of helicity accompanying the recombination process can be ruled out, and the helicity of the final helicate mirrors that of the original receptor.

Chiro-Optical Properties of *MM*-$(-)_{589}$-$[LnCr(L8)_3]^{6+}$ (Ln = Eu, *MM*-2; Ln = Gd, *MM*-3; Ln = Tb, *MM*-4) and *PP*-$(+)_{589}$-$[LnCr(L8)_3]^{6+}$ (Ln = Eu, *PP*-2; Ln = Gd, *PP*-3; Ln = Tb, *PP*-4). The specific rotary dispersions of *MM*-$(-)_{589}$-$[LnCr(L8)_3]^{6+}$ and *PP*-$(+)_{589}$-$[LnCr(L8)_3]^{6+}$ (Ln = Eu, Gd, Tb) display the expected opposite values within experimental error, but it is worth noting that the sign of $[\alpha]_{589}^{20}$ is inverted when going from the receptor *M*-$[Cr(L8)_3]^{3+}$ to the corresponding helicate *MM*-$[LnCr(L8)_3]^{6+}$, while the absolute specific rotations increase by approximately 30% (Table 3). This suggests that the complexation and helication of the tridentate binding units significantly contribute to the chiro-optical properties in $[LnCr(L8)_3]^{6+}$. Interestingly, the absolute values $892 \leq |[\alpha]_{589}^{20}| \leq 1239$ deg·mol^{-1}·dm^2 found for *PP*/*MM*-$[LnCr(L8)_3]^{6+}$ (Table 3) match $|[\alpha]_{589}^{20}| = 1080(10)$ deg·mol^{-1}·dm^2 reported for the closely related triple-stranded helicate *PP*/*MM*-$[Co_2(L9)_3]^{6+}$ in which three bis-bidentate segmental strands are wrapped around two Co(III) (Chart 2).[29] A slightly smaller specific

(29) Charbonnière, L. J.; Bernardinelli, G.; Piguet, C.; Sargeson, A. M.; Williams, A. F. *J. Chem. Soc., Chem. Commun.* **1994**, 1419.

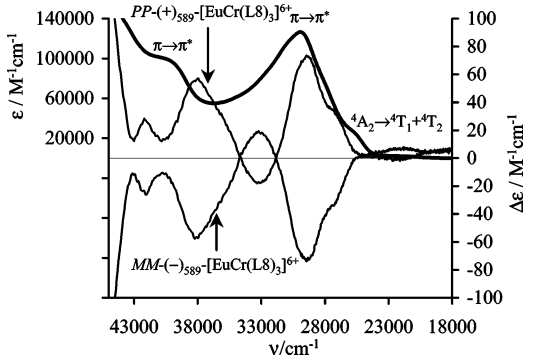

Figure 7. Absorption spectrum of $[EuCr(L8)_3]^{6+}$ (bold line, 10^{-3} M) and circular dichroism spectra of *MM*-$(-)_{589}$-$[EuCr(L8)_3]^{6+}$ and *PP*-$(+)_{589}$-$[EuCr(L8)_3]^{6+}$ (acetonitrile, 5×10^{-5} M, corrected for partial (23%) decomplexation of $[EuCr(L8)_3]^{6+}$ calculated with $\log(\beta_{11}^{Ln})$ given in Table 1).

rotary dispersion $[\alpha]_{589}{}^{20} = -600$ deg·mol^{-1}·dm^2 has been obtained for the monometallic triple-helical lanthanide complex $[Ln(L10)_3]^{3+}$ in which a single helical diastereomer exists in solution.[30] However, the faint rotary dispersions reported for $[Ln(S\text{-}L11)_3]^{3+}$ ($[\alpha]_{589}{}^{20} = -30$ deg·mol^{-1}·dm^2)[31] and $[Ln(S\text{-}L12)_3]^{3+}$ ($[\alpha]_{589}{}^{20} = 31$ deg·mol^{-1}·dm^2)[32] confirm the poor helical induction performed by the stereogenic carbon centers in these chiral ligands, which leads to the formation of a faint diastereomeric excess in solution.

Chart 2

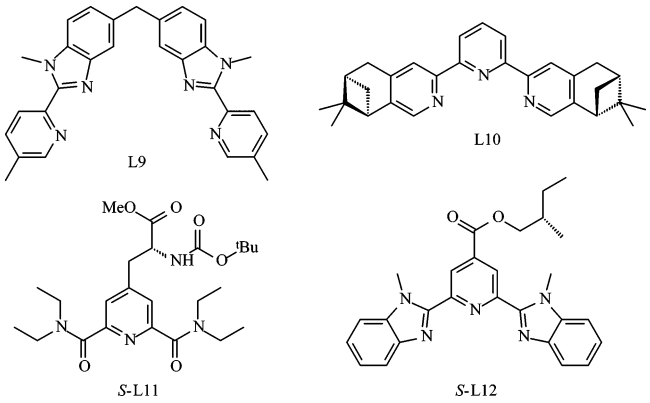

The circular dichroism spectra of the *MM*- and *PP*-$[LnCr(L8)_3]^{6+}$ in acetonitrile (18 000−45 000 cm^{-1} range) display the expected mirror images and are identical for Ln = Eu, Gd, and Tb (Figure 7 and Figures S4 and S5, Supporting Information). The $\pi \rightarrow \pi^*$ transitions produce six CD signals with strong Cotton effects, and comparison with the spectra of the chiral receptors *M*/*P*-$[Cr(L8)_3]^{3+}$(Figure 4) shows a completely different pattern because both the bidentate units coordinated to Cr(III) and the tridentate binding units coordinated to Ln(III) contribute to the CD spectra in *MM*/*PP*-$[LnCr(L8)_3]^{6+}$ (Figure S6, Supporting Information). This demonstrates that tentative assignments of the absolute

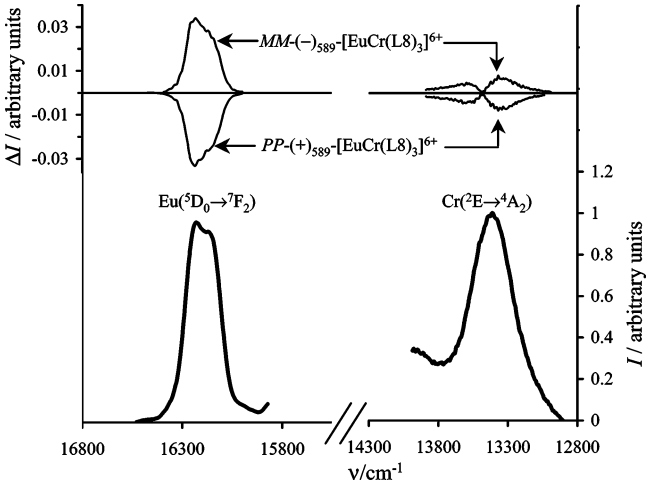

Figure 8. CPL spectra of the Eu($^5D_0 \rightarrow {}^7F_2$) and Cr($^2E \rightarrow {}^4A_2$) transitions for *MM*/*PP*-$[EuCr(L8)_3]^{6+}$ in acetonitrile (10^{-3} M, 295 K; $\nu_{exc} = 17238$ cm^{-1} for Eu($^5D_0 \rightarrow {}^7F_2$) and $\nu_{exc} = 20\,492$ cm^{-1} for Cr($^2E \rightarrow {}^4A_2$)).

configuration based on the exciton theory are strictly limited to the receptor *M*/*P*-$[Cr(L8)_3]^{3+}$ in which the overlapping $\pi \rightarrow \pi^*$ transitions centered on the noncoordinated tridentate binding units show only minor contributions to the total CD signal. The absolute value $|\Delta\epsilon_{max}| = 74$ M^{-1} cm^{-1} recorded at 29 410 cm^{-1} for *MM*/*PP*-$[LnCr(L8)_3]^{6+}$ (Figure 7) roughly correlates with $|\Delta\epsilon_{max}| = 22$ M^{-1} cm^{-1} recorded at 29 300 cm^{-1} for the triple-stranded helicates *PP*/*MM*-$[Co_2(L9)_3]^{6+}$ in which identical coordinated bidentate binding units are wrapped about the helical axis and contribute to the CD signal.[29]

Finally, we have resorted to circularly polarized luminescence (CPL) for quantitatively investigating the helical chirality on the polarized emission of the metal-centered Cr($^2E \rightarrow {}^4A_2$) and Eu($^5D_0 \rightarrow {}^7F_J$) ($J = 1, 2$) transitions observed in $[EuCr(L8)_3]^{6+}$.[12] The CPL observed for *MM*/*PP*-$[EuCr(L8)_3]^{6+}$ indeed reflects the geometry of the complex in its excited states,[33,34] but the emitting metal-centered excited states Cr(^2E)[35] and Eu($^5D_0$)[36] display geometries which are very similar to that found in the ground state since no electron is promoted into an antibonding orbital. Selective nonpolarized excitation of the Eu($^7F_0 \rightarrow {}^5D_0$) transition at 17 238 cm^{-1} or of the Cr($^4A_2 \rightarrow {}^4T_2$) transition at 20 492 cm^{-1} in *MM*-$[EuCr(L8)_3]^{6+}$ (10^{-3} M in acetonitrile, 298 K) produces small different intensities $\Delta I = I_L - I_R$ between the left (I_L) and right (I_R) components of the induced circularly polarized emission of the Cr($^2E \rightarrow {}^4A_2$) and Eu($^5D_0 \rightarrow {}^7F_2$) transitions (Figure 8). The exact mirror images obtained for the two enantiomers *MM*/*PP*-$[EuCr(L8)_3]^{6+}$ confirm their optical purity, and we calculate disymmetry factors of

(30) Muller, G.; Bünzli, J.-C. G.; Riehl, J. P.; Suhr, D.; von Zelewsky, A.; Mürner, H. *Chem. Commun.* **2002**, 1522.
(31) Muller, G.; Schmidt, B.; Jiricek, J.; Hopfgartner, G.; Riehl, J. P.; Bünzli, J.-C. G.; Piguet, C. *J. Chem. Soc., Dalton Trans.* **2001**, 2655.
(32) Muller, G.; Riehl, J. P.; Schenk, K. J.; Hopfgartner, G.; Piguet, C.; Bünzli, J.-C. G. *Eur. J. Inorg. Chem.* **2002**, 3101.
(33) (a) Riehl, J. P. In *Encyclopedia of spectroscopy and spectrometry*; Lindon, J. C., Tranter, G. E., Holmes, J. L., Eds.; Academic Press: San Diego, CA, 2000; pp 243−244. (b) Richardson, F. S. *Chem. Rev.* **1977**, *77*, 773. (c) Richardson, F. S. *Chem. Rev.* **1982**, *82*, 541. (d) Riehl, J. P.; Richardson, F. S. *Chem. Rev.* **1986**, *86*, 1.
(34) Riehl, J. P.; Muller, G. *Handbook on the Physics and Chemistry of Rare Earths*; Gschneidner, K. A., Bünzli, J.-C. G., Eds.; North-Holland Publishing Company: Amsterdam, submitted.
(35) Kirk, A. D. *Chem. Rev.* **1999**, *99*, 1607.
(36) Bünzli, J.-C. G. In *Lanthanide Probes in Life, Chemical and Earth Sciences*; Elsevier: Amsterdam, 1989; Chapter 7.

g_{lum}^{13423} {Cr($^2E \rightarrow {}^4A_2$)} = ±0.01 and g_{lum}^{16234} {Eu($^5D_0 \rightarrow {}^7F_2$)} = ±0.07 with eq 3.[1a,33,34]

$$g_{lum}^{\nu} = \frac{2\Delta I}{I} = \frac{2(I_L^{\lambda} - I_R^{\lambda})}{(I_L^{\lambda} + I_R^{\lambda})} \quad (3)$$

Since the detection of CPL signals for the magnetic-dipole Eu($^5D_0 \rightarrow {}^7F_1$) transitions is difficult upon selective excitation of the neighboring Eu($^7F_0 \rightarrow {}^5D_0$) transition, nonselective UV-irradiation of the ligand-centered $\pi \rightarrow \pi^*$ transitions have been attempted, despite the well-established fast photochemical degradation of [Cr(α,α-diimine)$_3$]$^{3+}$ occurring in these conditions, which may alter the sample.[35] Nevertheless, CPL data recorded immediately after irradiation at 28 249 cm^{-1} give g_{lum}^{16224} {Eu($^5D_0 \rightarrow {}^7F_1$)} = −0.154 for *MM*-[EuCr(L8)$_3$]$^{6+}$ and g_{lum}^{16224} {Eu($^5D_0 \rightarrow {}^7F_1$)} = +0.163 for *PP*-[EuCr(L8)$_3$]$^{6+}$. These values compare well with g_{lum}-{Eu($^5D_0 \rightarrow {}^7F_1$)} = 0.020 reported for [Eu(L10)$_3$]$^{3+}$ in which a single helical diastereomer exists in solution[30] and with g_{lum}{Eu($^5D_0 \rightarrow {}^7F_1$)} = −0.144 found for *P*-[Eu(oxydiacetate)$_3$]-Na$_3$ measured in the solid state.[37] In a complementary experiment, circularly left-polarized, and, respectively, right-polarized excitation of an acetonitrile solution of the racemic complex *rac*-[EuCr(L8)$_3$]$^{6+}$ produce dissymmetric factors (g_{lum}^{13423} {Cr($^2E \rightarrow {}^4A_2$)} = ±0.0006(1) and g_{lum}^{16234} {Eu($^5D_0 \rightarrow {}^7F_2$)} = ±0.0007(1)) which are 2 orders of magnitude smaller than those obtained for the pure enantiomeric analogues. This demonstrates that the diastereomeric excess induced in the excited states upon circularly polarized excitation remains weak compared to CPL signals obtained for pure chiral samples. Finally, CPL measurements performed with *MM*/*PP*-[GdCr(L8)$_3$]$^{6+}$ and *MM*/*PP*-[TbCr(L8)$_3$]$^{6+}$ show exclusively the polarized emission of Cr($^2E \rightarrow {}^4A_2$) (with g_{lum}^{16234} identical to those found for *MM*/*PP*-[EuCr(L8)$_3$]$^{6+}$) as a result of (i) the lack of accessible emitting state for Ln = Gd(III), and (ii) the quantitative Tb → Cr energy transfer previously evidenced in *rac*-[TbCr(L8)$_3$]$^{6+}$.[12]

Conclusion

The inert preorganized triple-helical receptor [Cr(L8)$_3$]$^{3+}$ offers a unique opportunity for preparing enantiomerically pure nonadentate podands in which helicity is the only source of chirality. Separation with $Na_2Sb_2[(+)\text{-}C_4O_6H_2]_2 \cdot 5H_2O$ is rather easy, and the subsequent recombination with a judicious Ln(III) cation opens the first efficient access to inert and enantiomerically pure triple-stranded lanthanide helicates with no stereogenic carbon center. The introduction of emissive Eu(III) in *MM*/*PP*-[EuCr(L8)$_3$]$^{6+}$ allows the simultaneous detection of circularly polarized luminescence for Eu- and Cr-centered transitions occurring at two different wavelengths and with specific lifetimes controlled by the intramolecular energy transfer processes involved in this supramolecular edifice.[12] Applications as sensors for chiral substrates with spatial and time resolution are thus an attractive perspective. These systems also contribute to improve the elaboration of possible correlations between molecular structures and CPL spectra which are currently lacking.[1a,33a,34] The disymmetry factors g_{lum} measured for *MM*/*PP*-[LnCr(L8)$_3$]$^{6+}$ eventually demonstrate that helicity is mainly responsible for the considerable Ln-centered chiro-optical properties previously reported for triple-helical[30,37] and quadruple-helical[1a,38] monometallic lanthanide complexes existing as single diastereomers, and whose absolute helicities are induced by a neighboring stereogenic carbon center. Interestingly, the quantitative comparison of g_{lum}{Eu($^5D_0 \rightarrow {}^7F_1$)} = +0.16 for *PP*-[EuCr(L8)$_3$]$^{6+}$ and g_{lum}{Eu($^5D_0 \rightarrow {}^7F_1$)} = +0.18 for *M*-[Eu(DOTMNpA)$_3$] (DOTMNpA is a DOTA platform grafted with four chiral secondary amide sidearms)[38] suggests that helicity is globally an efficient tool for inducing large CPL signals. Finally, the unambiguous assignment of the absolute configuration of *MM*-[EuCr(L8)$_3$]$^{6+}$ by X-ray diffraction techniques has initiated a detailed re-evaluation of possible correlations between the sign of the CPL obtained for the magnetic-dipole Eu($^5D_0 \rightarrow {}^7F_1$) transitions and their molecular origin which will be reported elsewhere.

Experimental Section

Solvents and Starting Materials. These were purchased from Fluka AG (Buchs, Switzerland) and Aldrich and used without further purification unless otherwise stated. The products *rac*-[LnCr(L8)$_3$](CF$_3$SO$_3$)$_6$·2H$_2$O[12] and $Na_2Sb_2[(+)\text{-}C_4O_6H_2]_2 \cdot 5H_2O$[16] were prepared according to literature procedures. The triflate salts Ln(CF$_3$SO$_3$)$_3$·xH$_2$O (Ln = La−Lu, Y; x = 1−4) were prepared from the corresponding oxides (Rhodia, 99.99%).[39] The Ln content of solid salts was determined by complexometric titrations with Titriplex III (Merck) in the presence of urotropine and xylene orange.[40] Acetonitrile was distilled over calcium hydride.

Preparation of *rac*-[Cr(L8)$_3$](CF$_3$SO$_3$)$_3$·4H$_2$O (1). A solution of 73 μmol of [(^{n}Bu)$_4$N]$_4$EDTA·6.4H$_2$O in acetonitrile (900 μL) was added to a solution of [LaCr(L8)$_3$](CF$_3$SO$_3$)$_6$·2H$_2$O (200 mg, 73 μmol) in acetonitrile (7 mL). The resulting white precipitate ([(^{n}Bu)$_4$N][La(EDTA)]) was removed by centrifugation and the remaining clear solution concentrated. Precipitation was induced by addition of diethyl ether, and the resulting mixture was frozen at −20 °C for one night. The cold precipitate was filtered and washed with diethyl ether. The same procedure (precipitation, freezing, and filtration) was repeated until complete removal of (^{n}Bu)$_4$N signals in ^{1}H NMR spectrum. The final separated solid was dried under vacuum at 40 °C overnight to yield 105.6 mg of [Cr(L8)$_3$](CF$_3$SO$_3$)$_3$·4H$_2$O (**1**: 48 μmol, yield 66%) as an orange powder. Elemental analysis calculated for $CrC_{102}H_{107}N_{21}O_{16}F_9S_3$: C 55.63, H 4.90, N 13.35. Found: C 55.89, H 4.98, N 13.33.

Optical Resolution of *M*/*P*-[Cr(L8)$_3$](CF$_3$SO$_3$)$_3$ (*M*-1 and *P*-1). A column of 1 cm diameter and 75 cm length was packed with 23 g of Sephadex-SP-C25 resin swollen in water. A 38 mg portion of [LaCr(L8)$_3$](CF$_3$SO$_3$)$_6$·2H$_2$O (13.8 μmol) mixed with a small quantity of resin and swollen in water was sorbed onto the column

(37) Morley, J. P.; Saxe, J. D.; Richardson, F. S. *Mol. Phys.* **1982**, *47*, 379.

(38) Dickens, R. S.; Howard, J. A. K.; Maupin, C. L.; Moloney, J. M.; Parker, D.; Peacock, R. D.; Riehl, J. P.; Siligardi, G. *New J. Chem.* **1998**, 891.

(39) Desreux, J.-F. In *Lanthanide Probes in Life, Chemical and Earth Sciences*; Bünzli, J.-C. G., Choppin, G. R., Eds.; Elsevier Publishing Co.: Amsterdam, 1989; Chapter 2, p 43.

(40) Schwarzenbach, G. *Complexometric Titrations*; Chapman & Hall: London, 1957; p 8.

and eluted with a 0.15 M aqueous solution of $Na_2Sb_2[(+)\text{-}C_4O_6H_2]_2\cdot 5H_2O$. The two resulting fractions were collected and extracted with dichloromethane after addition of CF_3SO_3Na. Organic solutions were evaporated and dried under vacuum to yield 13.2 mg of *P*-$(-)_{589}$-$[Cr(L8)_3](CF_3SO_3)_3\cdot H_2O$ (*P*-**1**, yield 45%) and 12.4 mg of *M*-$(+)_{589}$-$[Cr(L^5)_3]^{3+}(CF_3SO_3)_3\cdot 3H_2O$ (*M*-**1**, yield 41%). Elemental analyses calcd for *P*-$(-)_{589}$-$CrC_{102}H_{101}N_{21}O_{13}F_9S_3$: C 57.03, H 4.74, N 13.69. Found: C 57.12, H 4.95, N 13.05. Calcd for *M*-$(+)_{589}$-$CrC_{102}H_{105}N_{21}O_{15}F_9S_3$: C 56.09, H 4.85, N 13.47. Found: C 56.03, H 4.72, N 13.22.

Preparation of *MM*-$(-)_{589}$-$[LnCr(L8)_3](CF_3SO_3)_6\cdot xH_2O$ (Ln = Eu, *x* = 1, *MM*-2; Ln = Gd, *x* = 3, *MM*-3; Ln = Tb, *x* = 6.5, *MM*-4) and *PP*-$(+)_{589}$-$[LnCr(L8)_3](CF_3SO_3)_6\cdot xH_2O$ (Ln = Eu, *x* = 1.5, *PP*-2; Ln = Gd, *x* = 1.5, *PP*-3; Ln = Tb, *x* = 8, *PP*-4). To a solution of 39 mg (1.77×10^{-5} mol) of *M*-$(+)_{589}$-$[Cr(L8)_3](CF_3SO_3)_3\cdot 3H_2O$ in acetonitrile (2 mL) was added a solution of $Eu(CF_3SO_3)_3\cdot 4.1H_2O$ (11.9 mg, 1.77×10^{-5} mol) in acetonitrile (2 mL). The resulting solution was stirred for 1 h and evaporated to dryness. Fractionnal crystallization by diffusion of diethyl ether in a concentrated solution of acetonitrile allowed isolation of microcrystals which were collected by filtration and dried under vacuum at 40 °C overnight to yield 41.4 mg of *MM*-$(-)_{589}$-$[EuCr(L8)_3](CF_3SO_3)_6\cdot H_2O$ (*MM*-**2**: 15 μmol, 77%). This product was redissolved in acetonitrile for polarimetry, CD, and CPL measurements. The preparations of *MM*-**3**, *MM*-**4**, and, respectively, *PP*-**2**, *PP*-**3**, and *PP*-**4** were performed with the same procedure (yield 77−92%) by using *M*-$(+)_{589}$-$[Cr(L8)_3](CF_3SO_3)_3\cdot 3H_2O$ (*M*-**1**), and, respectively, *P*-$(-)_{589}$-$[Cr(L8)_3](CF_3SO_3)_3\cdot H_2O$ (*P*-**1**). All these complexes were characterized by their IR spectra and by elemental analyses (Table S1, Supporting Information). Ultra-slow diffusion of diethyl ether into a concentrated acetonitrile solution of *MM*-**2** provides fragile crystals of *MM*-$(-)_{589}$-$[EuCr(L8)_3](CF_3SO_3)_6\cdot 4CH_3CN$ (*MM*-**5**) suitable for X-ray diffraction studies.

Crystal-Structure Determination of *MM*-$(-)_{589}$-$[EuCr(L8)_3](CF_3SO_3)_6\cdot 4CH_3CN$ (*MM*-5). Crystal structure data follow: $EuCrC_{113}H_{111}N_{25}O_{21}S_6F_{18}$; $M_r = 2893.8$; $\mu = 0.786$ mm^{-1}, $d_x = 1.533$ g·cm^{-3}, monoclinic, $P2_1$, $Z = 2$, $a = 15.0152(8)$ Å, $b = 22.2897(10)$ Å, $c = 19.5322(10)$ Å, $\beta = 106.533(6)°$, $V = 6266.9(6)$ Å^3; yellow prism $0.13 \times 0.25 \times 0.28$ mm^3 mounted on a quartz fiber with protection oil. Cell dimensions and intensities were measured at 200 K on a Stoe IPDS diffractometer with graphite-monochromated Mo[Kα] radiation ($\lambda = 0.7107$ Å): 79 184 measured reflections, $2\theta_{max} = 51.8°$, 24 405 unique reflections of which 13 951 were observable ($|F_o| > 4\sigma(Fo)$); $R_{int} = 0.057$ for 54 740 equivalent reflections. Data were corrected for Lorentz and polarization effects and for absorption ($T_{min,max} = 0.8210, 0.9143$). The structure was solved by direct methods (SIR97);[41] all other calculations were performed with XTAL[42] system and ORTEP[43] programs. Full-matrix least-squares refinement based on *F* using weight of $1/(\sigma^2(F_o) + 0.0002(F_o^2))$ gave final values $R = 0.047$, $R_w = 0.044$, and $S = 1.92(1)$ for 1664 variables and 13 951 contributing reflections. Flack parameter[28] $x = -0.01(1)$. The final difference electron density map showed a maximum of +1.14 and a minimum of −2.57 e Å^{-3}. The hydrogen atoms were placed in calculated positions and contributed to F_c calculations. The triflate anions h and i were disordered and refined with restraints on bond distances and bond angles on two sites with population parameters of 0.75/0.25 (triflate h) and 0.60/0.40 (triflate i). The methyl groups C28b and C30c showed large atomic displacement parameters, but attempts to refine them on two different atomic sites did not improve convergence. CCDC-222420 contains the supplementary crystallographic data for *MM*-$[EuCr(L8)_3](CF_3SO_3)_6\cdot 4CH_3CN$ (*MM*-**5**). These data can be obtained free of charge via www.ccdc.cam.ac.uk/conts/retrieving.html (or from the Cambridge Crystallographic Data Centre, 12 Union Road, Cambridge CB2 1EZ, U.K.; fax: (+44) 1223-336-033; or deposit@ccdc.cam.ac.uk).

Spectroscopic and Analytical Measurements. Electronic spectra in the UV−vis were recorded at 293 K from 10^{-3} M solutions in acetonitrile with a Perkin-Elmer Lambda 900 spectrometer using quartz cells of 0.1 and 0.01 cm path length. IR spectra were obtained from KBr pellets with a Perkin-Elmer 883 spectrometer. Circular dichroism spectra were recorded at 293 K from $5-7 \times 10^{-5}$ M solutions in acetonitrile with a JASCO J-715 spectropolarimeter using quartz cells of 0.1 cm path length. Optical rotations were measured on a Perkin-Elmer 241 polarimeter using a quartz cell of 10 cm path length at 293 K with high-pressure lamps of sodium or mercury from 0.2 g·L^{-1} solutions in acetonitrile. CPL measurements were made on an instrument described previously, operating in a differential photon-counting mode.[33d,34] Pneumatically assisted electrospray (ESI-MS) mass spectra were recorded from 10^{-4} M acetonitrile solutions on a Finnigan SSQ 7000 instrument. ^{1}H NMR spectra were recorded at 298 K on a Broadband Varian Gemini 300 spectrometer. Chemical shifts are given in ppm vs TMS. Spectrophotometric titrations were performed in batch at 25 °C with a Perkin-Elmer Lambda 900 spectrometer using quartz cells of 0.1 cm path length. Acetonitrile solutions containing a total $[Cr(L8)_3]^{3+}$ concentration of 10^{-4} mol·dm^{-3} and variable concentrations of $Ln(CF_3SO_3)_3\cdot xH_2O$ ($Ln/[Cr(L8)_3]^{3+} = 0.1-2.5$, 40 samples) were left to equilibrate overnight at 298 K. The absorption spectrum of each sample was then recorded and transferred to the computer. Mathematical treatment of the spectrophotometric titrations was performed with factor analysis[44] and with the SPECFIT program.[24] Elemental analysis were performed by Dr. H. Eder from the Microchemical Laboratory of the University of Geneva.

Acknowledgment. This work is supported through grants from the Swiss National Science Foundation. We thank A. Maréchal for her technical support and Prof. S. Matile for using his equipments for the measurements of chiro-optical properties (polarimeter and CD spectrometer).

Supporting Information Available: Additional tables and figures. Crystallographic data in CIF format. This material is available free of charge via the Internet at http://pubs.acs.org.

IC035292U

(41) Altomare, A.; Burla, M. C.; Camalli, M.; Cascarano, G.; Giacovazzo, C.; Guagliardi, A.; Moliterni, A. G. G.; Polidori, G.; Spagna, R. *J. Appl. Crystallogr.* **1999**, *32*, 115.

(42) *XTAL 3.2, User's Manual*; Hall, S. R., Flack, H. D., Stewart, J. M., Eds.; Universities of Western Australia and Maryland, 1989.

(43) Johnson, C. K. *ORTEP II*; Report ORNL-5138; Oak Ridge National Laboratory: Oak Ridge, TN, 1976.

(44) Malinowski, E. R.; Howery, D. G. *Factor Analysis in Chemistry*; Wiley: New York, 1980.